

MI-Gen: Multiple Instance Generation of Pathology Reports for Gigapixel Whole-Slide Images

Pingyi Chen^{1,2}, Honglin Li^{1,2}, Chenglu Zhu², Sunyi Zheng², Lin Yang^{2*}

¹Zhejiang University, ²Westlake University

chenpingyi@westlake.edu.cn, yanglin@westlake.edu.cn

Abstract

Whole slide images are the foundation of digital pathology for the diagnosis and treatment of carcinomas. Writing pathology reports is laborious and error-prone for inexperienced pathologists. To reduce the workload and improve clinical automation, we investigate how to generate pathology reports given whole slide images. On the data end, we curated the largest WSI-text dataset (TCGA-PathoText). In specific, we collected nearly 10000 high-quality WSI-text pairs for visual-language models by recognizing and cleaning pathology reports which narrate diagnostic slides in TCGA. On the model end, we propose the multiple instance generative model (MI-Gen) which can produce pathology reports for gigapixel WSIs. We benchmark our model on the largest subset of TCGA-PathoText. Experimental results show our model can generate pathology reports which contain multiple clinical clues. Furthermore, WSI-text prediction can be seen as an approach of visual-language pre-training, which enables our model to be transferred to downstream diagnostic tasks like carcinoma grading and phenotyping. We observe that simple semantic extraction from the pathology reports can achieve the best performance (0.838 of F1 score) on BRCA subtyping without adding extra parameters or tricky fine-tuning. Our collected dataset and related code will all be publicly available.

1. Introduction

Whole-slide images (WSI) based diagnostic pathology is the foundation and gold standard for early tumor discovery and developing therapies. Due to the enormous size and large amount of heterogeneous information that exists in WSIs, the reading and interpretation of the slide usually necessitates specialized pathologists to complete a relatively reliable diagnosis. Recently, with the advancement

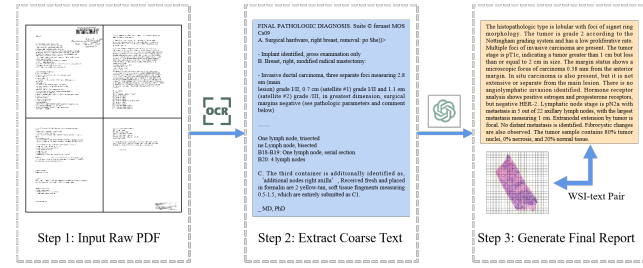


Figure 1. The pipeline of extracting WSI-text pairs from TCGA. We first get raw PDF files and then OCR is used to transform the characters into text. Finally, we resort to LLMs to summarize the text.

of the automation of WSIs, computational pathology has achieved remarkable success and, assisted with deep learning, some can even outperform experienced pathologists in certain tasks like tissue phenotyping [29, 35, 39, 47, 62], histological semantic segmentation [8, 34, 50, 52], and nuclei detection [1, 9, 44, 49]. These advanced methods have largely improved the automation of the pathological reading workflow, especially for those less-experienced pathologists in rural areas [63].

In spite of the "clinical-grade" performance of these computational pathology approaches, pathologists still need to organize the findings and write textual reports for each slide. Hundreds to thousands of WSIs need to be summarized in text in the pathology departments every day [17]. The automation of diagnostic reports can largely reduce the workload of pathologists. Furthermore, the content of pathology reports usually includes the diagnostic results previous pathological models can provide [7]. Therefore, it motivates us to take a step forward to achieve the automatic generation of pathology reports. On the data end, the great advancement of computational pathology in the past years owes very much to the emergence of publicly available pathology datasets. For example, The Cancer Genome Atlas (TCGA), as the largest cancer gene information database, contains at least 10,000 slides with associated

*Corresponding author.

clinical information from different centers. Many works of computational pathology rely on the subsets of TCGA to verify the effectiveness of their models [5, 11, 21, 27, 31]. However, there are few paired WSI-text datasets with public access due to privacy and some other reasons. And asking pathologists to annotate the existing public whole slide images is expensive and error-prone. To deal with the data shortage, some researchers resort to books, articles, and webs [18, 23, 40] to obtain large-scale image-text pairs. However, their collected texts are limited to patch-level descriptions. Furthermore, the correspondence between image and text is sometimes noisy and not well-aligned. Therefore, collecting high-quality WSI-text pairs is worth exploring and can boost the development of visual-language models in computational pathology.

We notice that TCGA includes scanning copies of pathology reports in the format of PDF¹. But they are too long with redundant information and present in a complex structure. Therefore, we propose a pipeline to extract and clean pathological texts from TCGA, which can convert complex PDF files to concise WSI-text pairs with the assistance of large language models (LLM), as shown in Fig. 1. The pairs we collected are also high-quality since they contain specialized knowledge from professional pathologists and have abundant clinical clues at slide-level, thus benefiting the construction of a more advanced visual-language model. To be specific, we first recognize WSI-PDF pairs from the TCGA dataset. Each pair contains a diagnostic whole slide image and its associated pathology report. We apply Optical Character Recognition (OCR) models [51] to extract text from the PDF files and obtain coarse reports. It is worth noting that OCR will transform all the characters in the PDF which inevitably results in text noise like page ID, signature, etc. Finally, we resort to LLMs like GPT-3.5-Turbo [6] to filter and summarize the coarse texts with prompts [37]. The proposed dataset is named as TCGA-PathoText containing total 9009 WSI-text pairs.

There are still challenges to achieving slide-level generation on the model end. Recent years have witnessed the boom of visual-language models in image captioning [46, 55, 59, 60]. And in the medical area, the generation of radiology reports has been explored by several works [12, 25, 36, 56]. However, the huge size of WSIs precludes existing machine learning techniques in image captioning from being transferred to the applications on WSIs. Existing image captioning methods for natural images and medical images all follow an end-to-end diagram where the entire image is encoded as the hidden state. It is unaffordable to directly process the WSIs with more than 10 gigapixels unless WSIs are resized or disentangled sacrificing much fine-grained information. In terms of the pathological approaches, PLIP [23] and MI-Zero [40] both adopt a

CLIP-like [45] structure which largely improves the zero-shot ability but is still unable to directly generate pathology reports. To deal with this problem, we introduce a **Multiple Instance Generation (MI-Gen)** framework to achieve WSI-based report generation. It contains a visual extractor which encodes the non-overlap patches with the sliding window and a sequence-to-sequence generator to produce pathology texts.

In this work, our contributions can be concluded as follows:

1. We propose a pipeline to curate high-quality WSI-text pairs from TCGA. The dataset (TCGA-PathoText) contains about ten thousand pairs which will be publicly accessible. It can potentially promote the development of visual-language models in pathology.
2. We design a multiple instance generation framework (MI-Gen). By incorporating the position-aware module, our model is more sensitive to the spatial information in WSIs.
3. We benchmark diverse sequence-to-sequence models on the subset of TCGA-PathoText. Downstream tasks are also included. As a generative model, our method is able to provide more abundant and accurate clinical results compared to previous MIL methods.

2. Related Works

2.1. Multiple Instance Learning for WSIs

Under multiple instance learning (MIL) frameworks, the slide is tiled where each small patch acts as an instance and the whole slide acts as a bag. Given only the bag label, the features of each instance are extracted and aggregated to make the prediction. MIL is essentially proposed to recognize the most relevant instance and thus previous works focus on the aggregation module. Wang et al. [57] adopted pooling operations to process instance features. They simply discard the less activated instance and keep the most discriminative one, which results in loss-of-details inevitably. Ilse et al. [24] proposed to use attention-weighted averaging as the aggregation operator. Chikontwe et al. [13] proposed a center loss to map the instance embeddings and reduce the intra-class variations. Some other works [48, 58, 62] specified the feature distances as attention scores and build convolutional neural networks to extract the instance-level correlation. Hou et al. [21] explicitly built the mutual-instance relationship of multi-resolution patches using a heterogeneous graph. Shao et al. [47] introduced the transformer-based model considering both the local context and the global correlation among the instances in the process of diagnosis. Our work also extracts features from non-overlap patches as individual instances from the whole bag.

¹<https://portal.gdc.cancer.gov/>

2.2. Image Captioning

The most related task to ours is image captioning where textual descriptions are generated automatically given images. Most image captioning models are characterized by the encoder-decoder structure. The encoder is used to extract features from the image followed by the decoder which generates captions in sequence. Many works adopt a CNN-RNN framework [16, 28, 41, 55]. Some other researchers have managed to incorporate attention mechanisms into the encoding of images [2, 38, 59, 60]. Recently, transformer-based models [14, 20, 22, 30] have emerged for their powerful representation power and parallel nature. Typically, they consist of an encoder with a stack of self-attention and a decoder that learns to allocate attention to image and word embeddings.

Medical visual-language models have also boomed for generating radiology reports. Different from the captions that narrate natural images, radiology reports are longer and contain many terminologies in certain patterns. Jing et al. [25] first investigated the generation of radiology reports in a multi-task learning framework. Yuan et al. [61] extended the generation pipeline by incorporating multi-view image fusion. To fully exploit the intrinsic characteristics of radiology reports, Li et al. [32] incorporated retrieval modules and Jing et al. [26] explored the structure information. Also, transformer models have been investigated. Chen et al. [12] proposed a memory-drive transformer to generate radiology reports. Miura et al. [42] proposed new rewards to generate factually complete and consistent reports. Tsuneki et al. [53] tried to caption the whole slide image. Their captions are somewhat short and the model they use is not so advanced. In our work, the captions we collected are longer and more like a report which tends to give a gross description of the slide.

3. Multiple Instance Generation: Problem Formulation

In the multiple instance generation framework, the huge image can be seen as a bag which contains a group of instances which are non-overlap patches with a much smaller resolution. Denote the cohort of instances as $Bag(X_i) = \{x_i^j\}_{j=1}^{M_i}$ where X_i is the i -th sample in the dataset and M_i is the sequence length which is determined by the patch size. Usually, when the patch size is 256, the sequence length M can be larger than ten thousand. A visual extractor h is adopted to extract image embeddings from the patches, denoted as $h(\{x_i^j\}) \in \mathbb{R}^{M_i \times l}$ where l is the embedding size.

A sequence-to-sequence model is incorporated to generate the target sequence $Y_i = \{y_i^j\}_{j=1}^{N_i}$ where N_i is the ground truth sequence length. Like previous text generation tasks, the encoder-decoder parameterized by ϕ is trained using language model objective which maximizes the sum

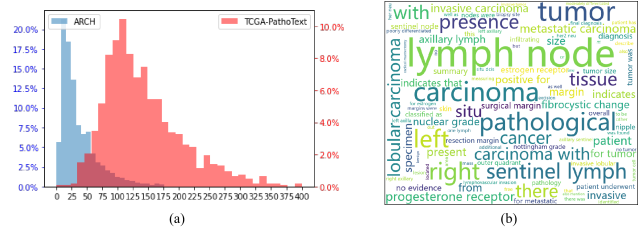


Figure 2. (a) Histogram of text lengths. It shows that TCGA-PathoText includes longer pathology reports compared to ARCH which only describes small patches. (b) Word cloud showing 100 most frequent tokens.

of conditional possibilities of individual words in the sequence. Therefore, the negative log-likelihood (NLL) loss can be calculated as:

$$L = - \sum_i^N \sum_{t=1}^N \log p_{\theta}(y_t | h(\{x_i^j\}), \{y_i^j\}_{j < t}; \phi). \quad (1)$$

The probability of j -th word is calculated based on the patch embeddings and the previous sequence $\{y_i^j\}_{j < t}$.

4. Method

4.1. TCGA-PathoText Construction

The first step in constructing TCGA-PathoText is to find out the diagnostic slides and their corresponding pathology reports in the TCGA. The diagnostic slides from TCGA cover diverse disease types originating at different primary sites. The pathology reports in the format of PDF usually contain multiple pages. We use OCR methods to transform the files into text. However, the text is still noisy because the report itself contains redundant information, and OCR sometimes generates garbled code. Therefore, we apply LLMs to filter and summarize the report. Given the prompt of "*Please summarize the following pathology report:*", the text is filtered and shortened for training. This pipeline is completely automatic without the need for labeling with experts.

TCGA-PathoText contains 9009 WSI-text pairs in total. Our collected text is distilled from clinical pathology reports with well-aligned correspondence and abundant pathological content. Therefore, our text is much longer than ARCH [18] (patch-level descriptions collected from books and articles) by the histogram of text lengths, as illustrated in Fig. 2. TCGA-PathoText is broken down into different subsets according to the disease type. For instance, TCGA-BRCA, which is the largest subset in TCGA, contains 1098 cases of breast cancer. The corresponding WSI-text subset in our TCGA-PathoText is named as TCGA-PathoText(BRCA). More details about TCGA-PathoText are demonstrated in the **Supplementary Materials**.

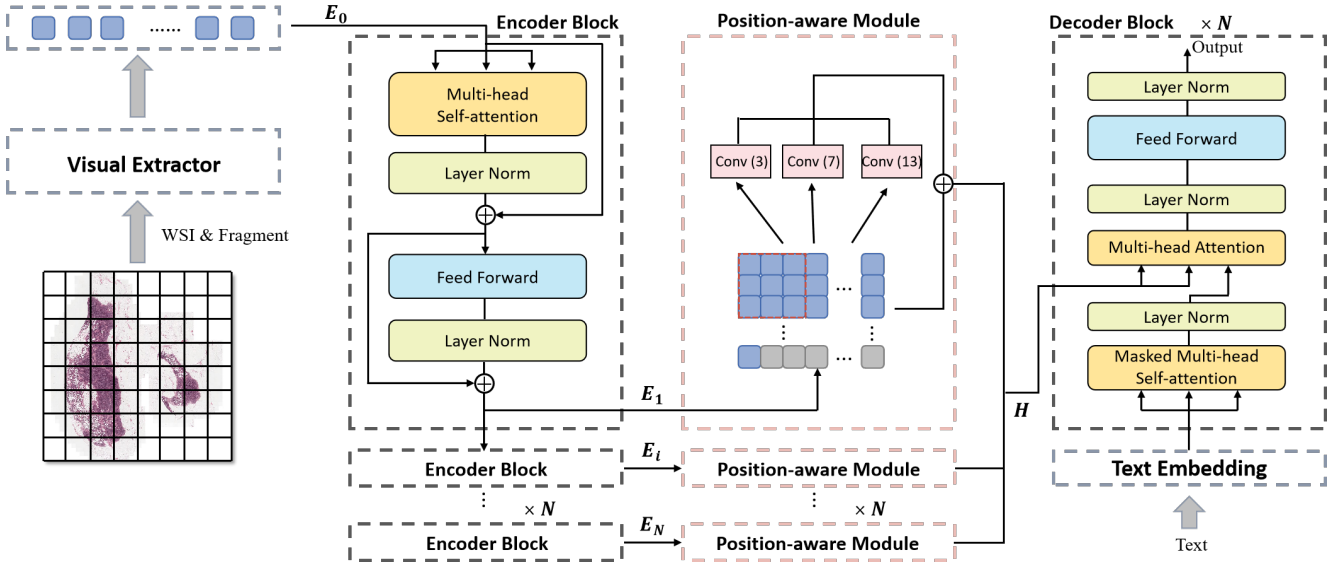


Figure 3. The framework of our proposed model is comprised of a visual extractor and an encoder-decoder. Firstly, we adopt a pre-trained visual extractor to transform WSI patches into embeddings. Distinct from standard Transformer, we also incorporate a Position-aware Module into the encoder to capture spatial information. The decoder is the same as the standard Transformer.

4.2. WSI-text Generation

As illustrated in Fig. 3, our proposed generative model consists of two parts: the visual extractor, and the encoder-decoder. We incorporate the hierarchical position-aware module into Transformer encoder layers so as to strengthen the model awareness of spatial information in WSIs. The details are described below.

4.2.1 Visual Extractor

Given a whole-slide image X_i with huge resolution, it is comprised of small patches $\{x_i^j\}_{j=1}^{M_i}$. It is unable to accumulate gradients in the visual extractor due to the large size of WSIs. Therefore, we apply pre-trained neural networks to extract features from these patches. The visual extractor is non-trainable during training. The initial image embeddings are denoted as E_0 which are fed to the subsequent modules.

4.2.2 Encoder-Decoder

Transformer has shown remarkable success in the past few years due to its strong capability of modeling the long sequence and interaction among individual tokens with self-attention. Therefore, we adopt Transformer as our backbone. Denote the Transformer encoder consists N transformer layers. The embeddings are processed by the transformer layers iteratively as:

$$E_i = f_i(E_{i-1}) \quad (2)$$

where $f_i(\cdot)$ refers to the i -th transformer layer. In standard Transformer, the hidden state of the last encoder layer E_N is directly fed to the cross-attention module with text embeddings for decoding. Whereas, we propose hierarchical position-aware modules to aggregate the embeddings from different encoder layers. The position-aware modules are inserted after each encoder layer so that more abundant context information is captured. Therefore, the hidden state H for decoding can be formulated as:

$$H = \sum_i PAM_i(E_i). \quad (3)$$

In terms of the decoder, we adopt the standard Transformer decoder where the inputs are the hidden state and text embeddings. In the training stage, a batch of samples is decoded in parallel with a subsequent mask. While in the inferring stage, the report is generated word by word. Therefore, the decoding will become more time-consuming if the target report is longer.

Position-aware Module. Morphological and spatial information plays a key role when pathologists are diagnosing WSIs. It has been confirmed in [47] that convolutional layers improve position information awareness. Inspired by this, we incorporate a hierarchical position-aware module (PAM) into the encoding of image embeddings. Considering the varying sizes of tokens in WSIs, we also conduct padding so that the feature map can be reshaped for fitting convolutional layers. Convolution kernels of various sizes are adopted to capture heterogeneous spatial information.

In specific, denote the sequence of image embeddings as

Visual Extractor & Pre-train	Encoder-Decoder	BLEU-1	BLEU-2	BLEU-3	BLEU-4	METEOR	ROUGE
ResNet&ImageNet	CNN-RNN[55]	0.334	0.209	0.122	0.074	0.137	0.248
	att-LSTM[59]	0.367	0.234	0.128	0.085	0.151	0.262
	vanilla Transformer [54]	0.395	0.230	0.135	0.089	0.145	0.254
	Mem-Transformer [12]	0.317	0.207	0.136	0.091	0.129	0.270
	Ours	0.403	0.254	0.168	0.117	0.163	0.280
ViT&ImageNet	CNN-RNN[55]	0.328	0.201	0.127	0.082	0.142	0.253
	att-LSTM[59]	0.341	0.211	0.132	0.083	0.145	0.265
	vanilla Transformer[54]	0.346	0.216	0.137	0.091	0.149	0.273
	Mem-Transformer[12]	0.332	0.216	0.144	0.100	0.147	0.268
	Ours	0.380	0.252	0.169	0.110	0.157	0.279
ViT&HIPT	CNN-RNN[55]	0.342	0.215	0.141	0.084	0.148	0.260
	att-LSTM[59]	0.372	0.230	0.135	0.090	0.150	0.269
	vanilla Transformer[54]	0.383	0.237	0.151	0.096	0.152	0.264
	Mem-Transformer[12]	0.344	0.218	0.150	0.103	0.151	0.268
	Ours	0.446	0.286	0.183	0.120	0.171	0.271

Table 1. Quantitative results of pathology report generation on TCGA-PathoText(BRCA). Different combinations of visual extractors and encoder-decoders are present for comparison. BLUE-n indicates the BLUE score computed based on n-grams.

$\mathbf{E}_i = \{e_j\}_{j=1}^{M_i}$. Firstly, we pad the sequence until its length becomes a square number T_i . Then, the 1-D sequence can be reshaped into 2-D space $\mathbf{E}_i^{pad} \in \mathbb{R}^{\sqrt{T_i} \times \sqrt{T_i} \times l}$. We adopt several CNNs to process and aggregate the 2-D embeddings:

$$PAM_i(\mathbf{E}_i) = \sum Conv_i(\mathbf{E}_i^{pad}) + \mathbf{E}_i^{pad}. \quad (4)$$

Heterogeneous spatial information from the CNNs with varying kernel sizes is summed together. Finally, the hidden state returns to 1-D space as a sequence for decoding. Our PAMs are inserted hierarchically after each encoder block, encoding abundant spatial information at different depth, which improves the awareness of spatial descriptions in the generated reports.

5. Experiments and Results

5.1. Implementation Details

Datasets. We train and validate our generative model on TCGA-PathoText(BRCA) which includes 845 pairs for training, 98 pairs for validating, and 98 pairs for testing. After training with WSI-text pairs from TCGA-PathoText, we evaluate the transfer performance on two WSI classification datasets: Camelyon-16 [4] for positive/negative binary classification and TCGA-BRCA for tumor subtyping. Camelyon-16 contains 400 hematoxylins and eosin (H&E) stained whole slide images for breast cancer. Our model is finetuned on the official training set of which 10% is randomly selected to constitute the validation set. TCGA-BRCA contains 1041 whole slide images with the label of invasive ductal (IDC) or invasive lobular carcinoma (ILC).

10% of TCGA-BRCA is randomly selected for validation and inference.

Model Setting. The number of encoder layers and decoder layers are both 3. For self-attention modules, the number of heads is 4 and the size of embeddings is 512. Three CNNs are adopted in the PAM with the kernel size of 3, 7, and 13 respectively. We use Adam with the learning rate of 1e-4 to optimize the model. The weight decay is 5e-5. We adopt beam search with the size of 3 as the sampling method. Our model is trained on four A100-80G GPUs.

5.2. Baselines

Considering the huge size of WSIs, the visual extractors are frozen during training. Therefore, the patch embeddings for text generation are fixed. To explore the effect of patch embeddings on the quality of generated text. We explore different pre-trained visual extractors. Two kinds of visual models are chosen as our visual extractor: ResNet [19] which is composed of convolutional layers and ViT [15] which is based on Transformer. The output of the visual extractor is the image features with the length of 1024 and 384 for ResNet and ViT respectively. For the pre-training of visual extractors, we explore two strategies: 1) ImageNet (out-of-domain) pre-training on extensive natural images, and 2) hierarchical self-supervised learning with a pyramid transformer (HIPT) [10] on TCGA (in-domain).

We compare our encoder-decoder with several popular image captioning methods. There are two models which decode by LSTMs: CNN-RNN [55] and att-LSTM [59]. We also re-implemented two state-of-the-art Transformer-based models. The first is Vanilla Transformer which can be seen as the ablated version of our method. The other is Mem-

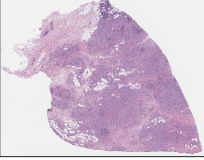
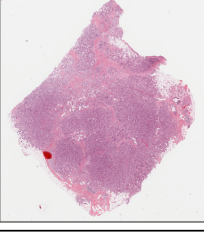
WSI	Ours	Vanilla Transformer	Ground-Truth
	<p><i>The pathological slide shows that the patient underwent a lumpectomy for invasive lobular carcinoma in the left breast. The tumor was identified as 2.6 cm in size and located on the boundary of the outer quadrants. There were no metastases in the axillary lymph nodes. The tumor has a mitotic rate of 5 mitoses per 10 high-power fields. Hormone receptors estrogen and progesterone receptors were found in over 75% of the tumor cells. The her2 protein was not detected in the invasive cancer cells.</i></p>	<p><i>The pathological slide shows that there is no tumor present in the left axillary lymph nodes. The left axillary sentinel lymph node no tumor present. The left axillary sentinel lymph node 3 no tumor present. The left breast mastectomy shows invasive lobular carcinoma. There is no tumor present. There is no tumor present in the nipple or skin. Lobular carcinoma in situ Ic is present. The tumor size of the invasive carcinoma is less than 0.1 cm. There is no tumor present. The resection margins are free of tumor. There is no tumor present in the axillary lymph nodes. No metastases of tumor is present in the axillary lymph nodes.</i></p>	<p><i>The pathological slide describes a left breast mastectomy with sentinel node biopsy. The right breast specimen showed no remarkable findings. The left breast specimen showed a 2.6 cm invasive lobular carcinoma with no lymph node involvement. The tumor was graded as nottingham grade 1 and had no involvement of the skin or nipple. The tumor was positive for estrogen and progesterone receptors and negative for her2. The margin of excision was negative for carcinoma.</i></p>
	<p><i>The pathological slide indicates that there is no tumor present in the lymph nodes examined. However a biopsy of the left breast shows the presence of invasive ductal carcinoma which is poorly differentiated. The invasive carcinoma measures 1.2 cm in size and extends to within 5.0 mm of the nearest deep margin. There is also the presence of ductal carcinoma comprising a solid type with necrosis which comprises less than 5% of the tumor area. All margins are free of tumor. Additional immunohistochemical stains and molecular pathologic assays have been requested for further analysis.</i></p>	<p><i>The pathological slide indicates that the patient has invasive ductal carcinoma in the right breast. The tumor has a nottingham grade 3 with a nuclear grade of 3 and a nuclear grade of there is no angiolymphatic invasion. The surrounding breast tissue shows the presence of ductal carcinoma in situ. The tumor measures 1.0 cm in its largest dimension. There is no lymphovascular space invasion. Resection margins are negative for tumor. The invasive tumor has a ductal carcinoma in situ high nuclear grade and ductal carcinoma in situ is also present. The resection margins are negative for invasive tumor. The resection margins are negative for tumor except for the presence of atypical ductal hyperplasia and fibrocytic changes with associated calcifications.</i></p>	<p><i>The pathological slide shows that a right-sided local excision was performed for a mass measuring 1.3 x 1.3 x 1.2 cm. The mass was diagnosed as invasive ductal carcinoma nottingham grade ii out of iii. There is also ductal carcinoma in situ comprising less than 5% of the tumor volume. No angiolymphatic invasion is present. Biopsy site changes were observed. All surgical resection margins are negative for tumor with a minimum tumor-free margin of 0.7 cm at the inferior margin. In addition, the slides states that multiple right axillary sentinel lymph nodes were examined and found to be negative for metastatic carcinoma.</i></p>
	<p><i>This is a pathological slide for a patient who underwent a radical mastectomy for a tumor in the breast. The tumor was identified as infiltrating ductal carcinoma moderately differentiated. The size of the tumor was 2.1 x 1.8 x 1.8 cm. No specific information was provided regarding the extent of the tumor or the margins. The nottingham histologic score which assesses various characteristics of the tumor could not be determined based on the provided information. There was no evidence of neo-adjuvant treatment or any additional pathologic findings.</i></p>	<p><i>The pathological slide indicates that the patient underwent a segmental mastectomy for a tumor in the breast. The tumor was identified as infiltrating ductal carcinoma moderately differentiated with a nottingham grade of there is no evidence of angiolymphatic invasion. The surgical margins are negative for tumor. The tumor is estrogen and progesterone receptors are negative. The tumor is negative for her-2. The final diagnosis is infiltrating ductal carcinoma of the tumor and lymph node metastasis.</i></p>	<p><i>The patient underwent a lumpectomy for a tumor in the breast. The tumor measured 2.1 x 1.8 x 1.4 cm and was identified as infiltrating ductal carcinoma. The tumor was moderately differentiated and the extent was not specified. There was no extracapsular invasion. The margins were uninvolved. The Nottingham Histologic Score indicated moderate tubule formation (score=2), marked nuclear pleomorphism (score=3), and a mitotic count of 10 to 20 mitoses per 10 high-power fields (score=2). The overall Nottingham Score was Grade II, indicating moderately differentiated cancer with a score of 6-7 points.</i></p>

Figure 4. Illustrations of pathology reports from our model, Vanilla Transformer, and ground-truth. The first column shows the thumbnails of the WSIs. The content that is consistent with the ground-truth is highlighted in bold. And the medical terms which are contradictory to ground-truth are underlined. Strikethrough text means there existing grammar errors.

Transformer [12] which is specially designed for medical report generation by incorporating a memory mechanism in the decoder.

5.3. Quantitative Results

As illustrated in Table 1, we adopt standard image captioning evaluation metrics to evaluate the generation performance: BLEU [43], METEOR [3], and ROUGE [33].

CNN-RNN adopts a standard encoder-decoder structure where images are first processed by convolutional layers and fed to an LSTM decoder for text generation. Att-LSTM adds an attention module between CNN and LSTM. We can observe that LSTM decoders perform relatively worse than transformer-based models. It shows the superiority of Transformer for modeling long sequences. Mem-Transformer incorporates the relational memory to implicitly model similar patterns in different reports. However, it does not show a better performance than Vanilla Transformer. The potential reason might be that pathology report in TCGA-PathoText is much longer than other medical image captioning datasets, thus having too heterogeneous structures to be memorized. In our model, we adopt hierarchical position-aware modules to capture spatial semantics

in the WSI. This mechanism facilitates our model to achieve the best performance no matter what the visual extractor is.

In terms of visual extractors, ResNet and ViT do not show a large difference when they are pre-trained on ImageNet. But ViT pre-trained with HIPT demonstrates a significant improvement. It is not surprising because domain-aligned pre-training usually outperforms out-of-domain ImageNet pre-training in pathology [27].

5.4. Qualitative Results

Three samples of WSIs with their corresponding pathology report from different models are illustrated in Figure 4. The first sentence is usually a general description of the WSI including the diagnosis of tumor subtype: "invasive lobular carcinoma" or "invasive lobular carcinoma". We can find that our model and Vanilla Transformer both give accurate subtyping results for these three WSIs. To further measure their ability of subtyping quantitatively, we go through all the generated reports and related results will be presented in the following section 5.5.

The pathology reports from ground-truth contain spatial information like tumor size ("2.6 cm", "1.3 x 1.3 x 1.2 cm"). Vanilla Transformer fails to give a tumor spatial description

(the first and third WSI) or generate not precise results (the second WSI), which reflects its disability to capture spatial features. Our model provides the perfectly right descriptions in the first and second row ("2.6 cm", "less than 5% of the tumor area") and partially correct results for the others ("1.2 cm", "2.1×1.8×1.8 cm"). The potential reason why 3-D size can not be accurately predicted may be that the WSI can only provide 2-D spatial information. For the first WSI, though ground-truth only presents positive/negative results for hormone receptors, our model still has the tendency to generate spatial descriptions ("75% of the tumor cells", "not detected"). Although it is impossible to check their correctness, the corresponding binary classification of these spatial descriptions is exactly right. This comparison demonstrates that position-aware modules largely improve the spatial awareness of our model.

Our model also generates more medical terms that are consistent with the ground-truth. Vanilla Transformer sometimes produces results that are not only inconsistent with the ground-truth but also self-contradictory, as shown in the first row ("There is no tumor present" following the claim of "invasive lobular carcinoma"). There are also repetitive sentences in reports from Vanilla Transformer. In terms of the Nottingham score of the third WSI, our model admits to being unable to make judgements. However, Vanilla Transformer generates text that is grammatically incorrect.

5.5. Transfer for WSI classification

Recent years have witnessed that large-scale visual-language pre-training benefits the performance on downstream tasks such as image classification [40, 45]. After training on the WSI-text pairs, we evaluate the transfer ability of our model on two WSI-level classification tasks: Camelyon-16 classification [4] and BRCA subtyping. We also re-produced several MIL approaches which are specially designed for WSI classification for comparison: AB-MIL [24], DS-MIL [29], CLAM-SB [39], and TransMIL [47]. They also segment the foreground regions and obtained pathological patches with a resolution of 256. These patches are transformed into embeddings by a visual extractor. For a fair comparison, we adopted the same ImageNet pre-trained ResNet-50 to extract image embeddings.

We adopt the encoder of our model with a trainable token attached at the head of the visual tokens. After encoding, this token is fed to a classifier to generate the classification result. Due to the existence of subtyping diagnosis in the text, we have also gone through all the reports and directly extracted semantic information for BRCA subtyping. Related results are demonstrated in Table 2. The first row is the result of the fully-supervised model which is trained under patch-level supervision so as to show the upper bound for the task.

Method	Dataset		Camelyon-16	TCGA-BRCA
	F1	AUC	F1	AUC
Fully-supervised	0.967	0.992	-	-
Max-pooling	0.805	0.824	0.644	0.826
AB-MIL [24]	0.828	0.851	0.771	0.869
DS-MIL [29]	0.857	0.892	0.775	0.875
CLAM-SB [39]	0.839	0.875	0.797	0.879
TransMIL [47]	0.846	0.883	0.806	0.889
Fine-tuning	0.841	0.855	0.780	0.897
Semantic Extraction	-	-	0.838	-

Table 2. The classification results on two breast cancer datasets. Different MIL approaches are included for comparison.

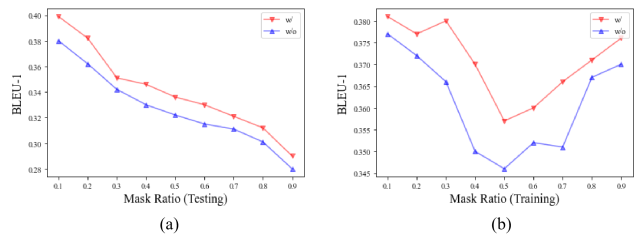


Figure 5. Effect of the position-aware module in training or testing with masked input. (a) shows the experiments where we conduct masking in the training stage, and (b) demonstrates the results when the test data is masked.

For the unseen domain Camelyon-16, our model can achieve a comparable performance. In terms of TCGA-BRCA subtyping, our model can achieve the best AUC performance by fine-tuning compared to other MIL baselines. It is worth noting that we can also obtain state-of-the-art classification results by simply extracting semantic information from the generated report without any additional parameters or training, which shows the potential of WSI-text generation in computational pathology.

5.6. Effect of Spatial Information

In the clinical scenario, an experienced pathologist allocates more attention to certain regions of interest instead of carefully checking all the patches in the WSIs. Therefore, to further analyze the robustness of our model and the proposed position-aware module, we add noise to the input by randomly masking some patches in the WSI. The quantitative results are demonstrated in Fig. 5: 'w/' represents our proposed model with position-aware modules while 'w/o' refers to the version without the position-aware module.

As shown in Fig. 5 (a), with the growth of mask ratio in test data, the performance drops continually. However, the performance of our model shows a consistent superiority over the model without the position-aware module. The position information contributes to an improvement of about

5% on BLEU-1 over text generation. When we conduct masking in the training stage, the overall performance does not show a consistent loss. Our model is more stable and still demonstrates its robustness. The spatial information enhances the model performance by around 3% of BLEU-1.

We also visualize the results, as illustrated in Fig. 6. The first column presents the masked WSIs with a higher mask ratio from top to down. We can observe that our model can maintain the report structure when the mask rate is low (0.3 and 0.5) sacrificing a little accuracy in tumor size identification (“ $2.2 \times 1.8 \times 1.8$ cm” versus “ $2.1 \times 1.8 \times 1.8$ cm”). At the same time, the version without position information fails to describe the size of the carcinoma and even grammar error appears. when the mask rate is very high (0.7 and 0.9), our model also fails to give a relatively accurate spatial description. And the model without position information generates more language-related errors. More ablation studies can be observed in **Supplementary Materials**.

6. Limitations and Future Work

Although it is a bit regretful that we are not able to train a universal model on the whole TCGA-PathoText due to the GPU limitation, we are still confident that our pipeline can be scaled to a larger domain. By bridging the gap among diverse disease types, we can obtain a more powerful pathological model in the future. In terms of the limitations of our model, we notice that the decoding time is long because the target report has many more tokens than patch-level descriptions. The average decoding time is nearly one hour for our validation set. Although it is clinically acceptable to wait for some time to receive the diagnosis results, we still hope to make decoding faster which at least helps to save costs when we are training at a very large-scale dataset. In addition, since the visual extractor is frozen during training, image embeddings and text embeddings may not be well-aligned. Visual features are either obtained from well-constructed backbones pre-trained on natural images or from self-supervised models pre-trained in pathology datasets. Since they are not adapted to the generative task, these task-agnostic features may hinder the performance.

7. Conclusion

In this paper, we have shown the feasibility of pathology report generation. On the data end, we collected nearly 10000 WSI-text pairs by transforming PDF files in TCGA into concise and comprehensive pathology reports with the aid of LLMs. Our proposed TCGA-PathoText is the largest WSI-text dataset so far to the best of our knowledge and is going to be available to the public. On the model end, we introduce MI-Gen as a generative model for WSI-level

Mask Ratio	w/	w/o	
		<p>This is a pathological slide for a patient who underwent a radical mastectomy for a tumor in the breast. The tumor was identified as infiltrating ductal carcinoma moderately differentiated. The size of the tumor was $2.1 \times 1.8 \times 1.8$ cm. No specific information was provided regarding the extent of the tumor or the margins. The nottingham histologic score which assesses various characteristics of the tumor could not be determined based on the provided information. There was no evidence of neo-adjuvant treatment or any additional pathologic findings.</p>	<p>The pathological slide indicates that the patient underwent a segmental mastectomy for a tumor in the breast. The tumor was identified as infiltrating ductal carcinoma moderately differentiated with a nottingham grade of 3. There is no evidence of angiolympathic invasion. The estrogen receptor and progesterone receptor are negative. The tumor is negative for her-2. The final diagnosis is infiltrating ductal carcinoma of the tumor and lymph node metastasis.</p>
0.3		<p>This is a pathological slide for a patient who underwent a radical mastectomy for a tumor in the breast. The tumor was identified as infiltrating ductal carcinoma moderately differentiated with a nottingham grade of $2.2 \times 1.8 \times 1.8$ cm. No specific information was provided regarding the extent of the tumor or the margins. The nottingham histologic score which assesses various characteristics of the tumor could not be determined based on the provided information. There was no evidence of neo-adjuvant treatment or any additional pathologic findings.</p>	<p>The pathological slide indicates the presence of invasive ductal carcinoma in the left breast. The tumor is invasive and has a size of 3.5 cm. There is also ductal carcinoma in situ (DCIS) present with nuclear grade 3 and a nottingham type necrosis and nuclear grade. The estrogen receptor and progesterone receptor are negative for carcinoma. The invasive tumor is estrogen receptor and progesterone receptor are negative for her-2. The pathological staging is pt2 no regional lymph node metastasis. The gross description of the specimen is provided.</p>
0.5		<p>This is a pathological slide for a patient who underwent a radical mastectomy for a tumor in the breast. The tumor was identified as infiltrating ductal carcinoma moderately differentiated. The size of the tumor was $2.1 \times 1.8 \times 1.8$ cm. No specific information was provided regarding the extent of the tumor or the margins. The nottingham histologic score which assesses various characteristics of the tumor could not be determined based on the provided information. There was no evidence of neo-adjuvant treatment or any additional pathologic findings.</p>	<p>The pathological slide indicates the presence of invasive ductal carcinoma in the right breast. The tumor is invasive and has a size of 3 with a nottingham grade of 3 and a nuclear grade 3. There is also ductal carcinoma in situ (DCIS) present with necrosis and calcifications. The resection margins are negative for tumor. The invasive tumor is located in the upper outer quadrant at the posterior margin. The resection margins are negative for tumor. Estrogen and progesterone receptors are positive.</p>
0.7		<p>The pathological slide indicates that the patient had a right breast mass which was found to be infiltrating ductal carcinoma with a prominent cribriform pattern. The tumor size in the biopsy specimen was $2.1 \times 1.8 \times 1.8$ cm. The tumor was located in the upper outer quadrant of the breast. There was no evidence of multifocality or in-situ carcinoma. The surgical margins were negative and no sentinel lymph nodes were examined. Nine lymph nodes were examined and no carcinoma was identified. Further testing for estrogen/progesterone receptors and cell cycle analysis is pending. The overall tumor size is estimated to be around 9 cm.</p>	<p>The pathological slide indicates that the patient has invasive ductal carcinoma in the right breast with a tumor diameter of 2.8 cm. The tumor is classified as grade 3 with no evidence of ductal carcinoma in situ (DCIS) present. The resection margins are negative for tumor. The invasive tumor is located in the upper outer quadrant at the posterior margin. The resection margins are positive. The tumor is positive for estrogen and progesterone receptors and negative for her-2. The slide also mentions the presence of invasive carcinoma in the ductal carcinoma with mucinous features. The tumor staging is pt2 no distant metastasis.</p>
0.9		<p>The pathological slide indicates that the patient has been diagnosed with invasive ductal carcinoma in the right breast. The tumor is small measuring 2.5 cm and is located near the upper quadrants of the breast. Within the tumor there are areas of high-grade carcinoma in situ (DCIS) intermediate nuclear grade comprising less than 5% of the total tumor volume. There is also evidence of angiolympathic invasion. The surrounding non-neoplastic breast tissue shows prominent areas of calcification. Calcifications are present in benign ducts and acini. The biopsy site shows changes but the surgical margins are negative for tumor. One of the three axillary sentinel lymph nodes that were removed is positive for metastatic carcinoma measuring 0.6 mm. There is no extramammary extension. A nevus is present in the skin of the right chest wall.</p>	<p>The pathological slide indicates the presence of invasive ductal carcinoma in the left breast with a tumor diameter of 2.8 cm. The tumor is classified as grade 3 with no evidence of ductal carcinoma in situ. The resection margins are negative for tumor. The invasive tumor is estrogen receptor and progesterone receptor positive. The tumor is classified as invasive ductal carcinoma with a grade of 3 and a high grade of there is no evidence of lymph node involvement. No distant metastasis is reported. The pathological staging is pt2.</p>

Figure 6. Effect of the position-aware module in testing with masked input. The first column shows the thumbnails of masked WSIs. The second column presents the reports generated from our model and the final column shows the results from the ablated version.

descriptions. By benchmarking different baselines on the subset of TCGA-PathoText, we also reveal the superiority of our model in being aware of the spatial information among the WSIs. Furthermore, the transfer performance on BRCA subtyping reflects the advancement of WSI-text generation since the pathology reports contain diverse clinical clues which have covered previous discriminative tasks. Many directions deserve exploring in the future including considering more WSI-text pairs, improving the alignment of visual and textual embeddings, and boosting the decoding efficiency in text generation. In addition, other fields that utilize high-resolution images like remote sensing can be inspired by our work.

References

[1] Shahira Abousamra, David Belinsky, John Van Arnam, Felicia Allard, Eric Yee, Rajarsi Gupta, Tahsin Kurc, Dimitris Samaras, Joel Saltz, and Chao Chen. Multi-class cell detection using spatial context representation. In *Proceedings of the IEEE/CVF International Conference on Computer Vision*, pages 4005–4014, 2021. 1

[2] Peter Anderson, Xiaodong He, Chris Buehler, Damien Teney, Mark Johnson, Stephen Gould, and Lei Zhang. Bottom-up and top-down attention for image captioning and visual question answering. In *2018 IEEE/CVF Conference on Computer Vision and Pattern Recognition*, pages 6077–6086, 2018. 3

[3] Satanjeev Banerjee and Alon Lavie. Meteor: An automatic metric for mt evaluation with improved correlation with human judgments. In *Proceedings of the acl workshop on intrinsic and extrinsic evaluation measures for machine translation and/or summarization*, pages 65–72, 2005. 6

[4] Babak Ehteshami Bejnordi, Mitko Veta, Paul Johannes Van Diest, Bram Van Ginneken, Nico Karssemeijer, Geert Litjens, Jeroen AWM Van Der Laak, Meyke Hermsen, Quirine F Manson, Maschenka Balkenhol, et al. Diagnostic assessment of deep learning algorithms for detection of lymph node metastases in women with breast cancer. *Jama*, 318(22):2199–2210, 2017. 5, 7

[5] Benjamin Bergner, Christoph Lippert, and Aravindh Mahendran. Iterative patch selection for high-resolution image recognition. *arXiv preprint arXiv:2210.13007*, 2022. 2

[6] Tom Brown, Benjamin Mann, Nick Ryder, Melanie Subbiah, Jared D Kaplan, Prafulla Dhariwal, Arvind Neelakantan, Pranav Shyam, Girish Sastry, Amanda Askell, et al. Language models are few-shot learners. *Advances in neural information processing systems*, 33:1877–1901, 2020. 2

[7] Julliette M Buckley, Suzanne B Coopey, John Sharko, Fernanda Polubriaginof, Brian Drohan, Ahmet K Belli, Elizabeth MH Kim, Judy E Garber, Barbara L Smith, Michele A Gadd, et al. The feasibility of using natural language processing to extract clinical information from breast pathology reports. *Journal of pathology informatics*, 3(1):23, 2012. 1

[8] Lyndon Chan, Mahdi S Hosseini, Corwyn Rowsell, Konstantinos N Plataniotis, and Savvas Damaskinos. Histosegnet: Semantic segmentation of histological tissue type in whole slide images. In *Proceedings of the IEEE/CVF International Conference on Computer Vision*, pages 10662–10671, 2019. 1

[9] Pingyi Chen, Chenglu Zhu, Zhongyi Shui, Jiatong Cai, Sunyi Zheng, Shichuan Zhang, and Lin Yang. Exploring unsupervised cell recognition with prior self-activation maps. In *Medical Image Computing and Computer Assisted Intervention – MICCAI 2023*, pages 559–568, Cham, 2023. Springer Nature Switzerland. 1

[10] Richard J Chen, Chengkuan Chen, Yicong Li, Tiffany Y Chen, Andrew D Trister, Rahul G Krishnan, and Faisal Mahmood. Scaling vision transformers to gigapixel images via hierarchical self-supervised learning. In *Proceedings of the IEEE/CVF Conference on Computer Vision and Pattern Recognition*, pages 16144–16155, 2022. 5

[11] Yuan-Chih Chen and Chun-Shien Lu. Rankmix: Data augmentation for weakly supervised learning of classifying whole slide images with diverse sizes and imbalanced categories. In *Proceedings of the IEEE/CVF Conference on Computer Vision and Pattern Recognition*, pages 23936–23945, 2023. 2

[12] Zhihong Chen, Yan Song, Tsung-Hui Chang, and Xiang Wan. Generating radiology reports via memory-driven transformer. In *Proceedings of the 2020 Conference on Empirical Methods in Natural Language Processing*, 2020. 2, 3, 5, 6

[13] Philip Chikontwe, Meejeong Kim, Soo Jeong Nam, Heoun-jeong Go, and Sang Hyun Park. Multiple instance learning with center embeddings for histopathology classification. In *International Conference on Medical Image Computing and Computer-Assisted Intervention*, pages 519–528. Springer, 2020. 2

[14] Marcella Cornia, Matteo Stefanini, Lorenzo Baraldi, and Rita Cucchiara. Meshed-Memory Transformer for Image Captioning. In *Proceedings of the IEEE/CVF Conference on Computer Vision and Pattern Recognition*, 2020. 3

[15] Alexey Dosovitskiy, Lucas Beyer, Alexander Kolesnikov, Dirk Weissenborn, Xiaohua Zhai, Thomas Unterthiner, Mostafa Dehghani, Matthias Minderer, Georg Heigold, Sylvain Gelly, et al. An image is worth 16x16 words: Transformers for image recognition at scale. *arXiv preprint arXiv:2010.11929*, 2020. 5

[16] Hao Fang, Saurabh Gupta, Forrest Iandola, Rupesh K Srivastava, Li Deng, Piotr Dollár, Jianfeng Gao, Xiaodong He, Margaret Mitchell, John C Platt, et al. From captions to visual concepts and back. In *Proceedings of the IEEE conference on computer vision and pattern recognition*, pages 1473–1482, 2015. 3

[17] Navid Farahani, Anil V Parwani, and Liron Pantanowitz. Whole slide imaging in pathology: advantages, limitations, and emerging perspectives. *Pathology and Laboratory Medicine International*, pages 23–33, 2015. 1

[18] Jevgenij Gamper and Nasir Rajpoot. Multiple instance captioning: Learning representations from histopathology textbooks and articles. In *Proceedings of the IEEE/CVF conference on computer vision and pattern recognition*, pages 16549–16559, 2021. 2, 3

[19] Kaiming He, Xiangyu Zhang, Shaoqing Ren, and Jian Sun. Deep residual learning for image recognition. In *Proceedings of the IEEE conference on computer vision and pattern recognition*, pages 770–778, 2016. 5

[20] Simao Herdade, Armin Kappeler, Kofi Boakye, and Joao Soares. Image captioning: Transforming objects into words. In *Advances in Neural Information Processing Systems*. Curran Associates, Inc., 2019. 3

[21] Wentai Hou, Lequan Yu, Chengxuan Lin, Helong Huang, Rongshan Yu, Jing Qin, and Liansheng Wang. H^2 2-mil: Exploring hierarchical representation with heterogeneous multiple instance learning for whole slide image analysis. In *Proceedings of the AAAI conference on artificial intelligence*, pages 933–941, 2022. 2

[22] L. Huang, W. Wang, J. Chen, and X. Wei. Attention on attention for image captioning. In *2019 IEEE/CVF International*

Conference on Computer Vision (ICCV), pages 4633–4642, Los Alamitos, CA, USA, 2019. IEEE Computer Society. 3

[23] Zhi Huang, Federico Bianchi, Mert Yuksekgonul, Thomas J Montine, and James Zou. A visual–language foundation model for pathology image analysis using medical twitter. *Nature medicine*, 29(9):2307–2316, 2023. 2

[24] Maximilian Ilse, Jakub Tomczak, and Max Welling. Attention-based deep multiple instance learning. In *International conference on machine learning*, pages 2127–2136. PMLR, 2018. 2, 7

[25] Baoyu Jing, Pengtao Xie, and Eric Xing. On the automatic generation of medical imaging reports. In *Proceedings of the 56th Annual Meeting of the Association for Computational Linguistics (Volume 1: Long Papers)*, pages 2577–2586, Melbourne, Australia, 2018. Association for Computational Linguistics. 2, 3

[26] Baoyu Jing, Zeyu Wang, and Eric Xing. Show, describe and conclude: On exploiting the structure information of chest X-ray reports. In *Proceedings of the 57th Annual Meeting of the Association for Computational Linguistics*, pages 6570–6580. Association for Computational Linguistics, 2019. 3

[27] Mingu Kang, Heon Song, Seonwook Park, Donggeun Yoo, and Sérgio Pereira. Benchmarking self-supervised learning on diverse pathology datasets. In *Proceedings of the IEEE/CVF Conference on Computer Vision and Pattern Recognition*, pages 3344–3354, 2023. 2, 6

[28] Andrej Karpathy and Li Fei-Fei. Deep visual-semantic alignments for generating image descriptions. In *Proceedings of the IEEE conference on computer vision and pattern recognition*, pages 3128–3137, 2015. 3

[29] Bin Li, Yin Li, and Kevin W Eliceiri. Dual-stream multiple instance learning network for whole slide image classification with self-supervised contrastive learning. In *Proceedings of the IEEE/CVF conference on computer vision and pattern recognition*, pages 14318–14328, 2021. 1, 7

[30] Guang Li, Linchao Zhu, Ping Liu, and Yi Yang. Entangled transformer for image captioning. *2019 IEEE/CVF International Conference on Computer Vision (ICCV)*, pages 8927–8936, 2019. 3

[31] Honglin Li, Chenglu Zhu, Yunlong Zhang, Yuxuan Sun, Zhongyi Shui, Wenwei Kuang, Sunyi Zheng, and Lin Yang. Task-specific fine-tuning via variational information bottleneck for weakly-supervised pathology whole slide image classification. In *Proceedings of the IEEE/CVF Conference on Computer Vision and Pattern Recognition*, pages 7454–7463, 2023. 2

[32] Yuan Li, Xiaodan Liang, Zhiting Hu, and Eric P Xing. Hybrid retrieval-generation reinforced agent for medical image report generation. In *Advances in Neural Information Processing Systems*. Curran Associates, Inc., 2018. 3

[33] Chin-Yew Lin. Rouge: A package for automatic evaluation of summaries. In *Text summarization branches out*, pages 74–81, 2004. 6

[34] Huangjing Lin, Hao Chen, Simon Graham, Qi Dou, Nasir Rajpoot, and Pheng-Ann Heng. Fast scannet: Fast and dense analysis of multi-gigapixel whole-slide images for cancer metastasis detection. *IEEE transactions on medical imaging*, 38(8):1948–1958, 2019. 1

[35] Tiancheng Lin, Zhimiao Yu, Hongyu Hu, Yi Xu, and Chang-Wen Chen. Interventional bag multi-instance learning on whole-slide pathological images. In *Proceedings of the IEEE/CVF Conference on Computer Vision and Pattern Recognition*, pages 19830–19839, 2023. 1

[36] Guanxiong Liu, Tzu-Ming Harry Hsu, Matthew McDermott, Willie Boag, Wei-Hung Weng, Peter Szolovits, and Marzyeh Ghassemi. Clinically accurate chest x-ray report generation. In *Machine Learning for Healthcare Conference*, pages 249–269. PMLR, 2019. 2

[37] Pengfei Liu, Weizhe Yuan, Jinlan Fu, Zhengbao Jiang, Hiroaki Hayashi, and Graham Neubig. Pre-train, prompt, and predict: A systematic survey of prompting methods in natural language processing. *ACM Computing Surveys*, 55(9):1–35, 2023. 2

[38] Jiasen Lu, Caiming Xiong, Devi Parikh, and Richard Socher. Knowing when to look: Adaptive attention via a visual sentinel for image captioning. In *2017 IEEE Conference on Computer Vision and Pattern Recognition (CVPR)*, pages 3242–3250, 2017. 3

[39] Ming Y Lu, Drew FK Williamson, Tiffany Y Chen, Richard J Chen, Matteo Barbieri, and Faisal Mahmood. Data-efficient and weakly supervised computational pathology on whole-slide images. *Nature biomedical engineering*, 5(6):555–570, 2021. 1, 7

[40] Ming Y Lu, Bowen Chen, Andrew Zhang, Drew FK Williamson, Richard J Chen, Tong Ding, Long Phi Le, Yung-Sung Chuang, and Faisal Mahmood. Visual language pre-trained multiple instance zero-shot transfer for histopathology images. In *Proceedings of the IEEE/CVF Conference on Computer Vision and Pattern Recognition*, pages 19764–19775, 2023. 2, 7

[41] Junhua Mao, Wei Xu, Yi Yang, Jiang Wang, Zhiheng Huang, and Alan Yuille. Deep captioning with multimodal recurrent neural networks (m-rnn). *arXiv preprint arXiv:1412.6632*, 2014. 3

[42] Yasuhide Miura, Yuhao Zhang, Emily Tsai, Curtis Langlotz, and Dan Jurafsky. Improving factual completeness and consistency of image-to-text radiology report generation. In *Proceedings of the 2021 Conference of the North American Chapter of the Association for Computational Linguistics: Human Language Technologies*, Online, 2021. Association for Computational Linguistics. 3

[43] Kishore Papineni, Salim Roukos, Todd Ward, and Wei-Jing Zhu. Bleu: a method for automatic evaluation of machine translation. In *Proceedings of the 40th annual meeting of the Association for Computational Linguistics*, pages 311–318, 2002. 6

[44] Hui Qu, Pengxiang Wu, Qiaoying Huang, Jingru Yi, Zhen-nan Yan, Kang Li, Gregory M. Riedlinger, Subhajyoti De, Shaoting Zhang, and Dimitris N. Metaxas. Weakly Supervised Deep Nuclei Segmentation Using Partial Points Annotation in Histopathology Images. *IEEE transactions on medical imaging*, 39(11):3655–3666, 2020. 1

[45] Alec Radford, Jong Wook Kim, Chris Hallacy, Aditya Ramesh, Gabriel Goh, Sandhini Agarwal, Girish Sastry, Amanda Askell, Pamela Mishkin, Jack Clark, et al. Learning

transferable visual models from natural language supervision. In *International conference on machine learning*, pages 8748–8763. PMLR, 2021. 2, 7

[46] Steven J Rennie, Etienne Marcheret, Youssef Mroueh, Jerret Ross, and Vaibhava Goel. Self-critical sequence training for image captioning. In *Proceedings of the IEEE conference on computer vision and pattern recognition*, pages 7008–7024, 2017. 2

[47] Zhuchen Shao, Hao Bian, Yang Chen, Yifeng Wang, Jian Zhang, Xiangyang Ji, et al. Transmil: Transformer based correlated multiple instance learning for whole slide image classification. *Advances in Neural Information Processing Systems*, 34:2136–2147, 2021. 1, 2, 4, 7

[48] Yash Sharma, Aman Shrivastava, Lubaina Ehsan, Christopher A Moskaluk, Sana Syed, and Donald Brown. Cluster-to-conquer: A framework for end-to-end multi-instance learning for whole slide image classification. In *Medical Imaging with Deep Learning*, pages 682–698. PMLR, 2021. 2

[49] Zhongyi Shui, Shichuan Zhang, Chenglu Zhu, Bingchuan Wang, Pingyi Chen, Sunyi Zheng, and Lin Yang. End-to-end cell recognition by point annotation. In *Medical Image Computing and Computer Assisted Intervention – MICCAI 2022*, pages 109–118, Cham, 2022. Springer Nature Switzerland. 1

[50] Korsuk Sirinukunwattana, Josien PW Pluim, Hao Chen, Xiaojuan Qi, Pheng-Ann Heng, Yun Bo Guo, Li Yang Wang, Bogdan J Matuszewski, Elia Bruni, Urko Sanchez, et al. Gland segmentation in colon histology images: The glas challenge contest. *Medical image analysis*, 35:489–502, 2017. 1

[51] Ray Smith. An overview of the tesseract ocr engine. In *Ninth international conference on document analysis and recognition (ICDAR 2007)*, pages 629–633. IEEE, 2007. 2

[52] Hiroki Tokunaga, Yuki Teramoto, Akihiko Yoshizawa, and Ryoma Bise. Adaptive weighting multi-field-of-view cnn for semantic segmentation in pathology. In *Proceedings of the IEEE/CVF Conference on Computer Vision and Pattern Recognition*, pages 12597–12606, 2019. 1

[53] Masayuki Tsuneki and Fahdi Kanavati. Inference of captions from histopathological patches. In *International Conference on Medical Imaging with Deep Learning*, pages 1235–1250. PMLR, 2022. 3

[54] Ashish Vaswani, Noam Shazeer, Niki Parmar, Jakob Uszkoreit, Llion Jones, Aidan N Gomez, Łukasz Kaiser, and Illia Polosukhin. Attention is all you need. *Advances in neural information processing systems*, 30, 2017. 5

[55] Oriol Vinyals, Alexander Toshev, Samy Bengio, and Dumitru Erhan. Show and tell: A neural image caption generator. In *Proceedings of the IEEE conference on computer vision and pattern recognition*, pages 3156–3164, 2015. 2, 3, 5

[56] Sheng Wang, Zihao Zhao, Xi Ouyang, Qian Wang, and Dinggang Shen. Chatcad: Interactive computer-aided diagnosis on medical image using large language models. *arXiv preprint arXiv:2302.07257*, 2023. 2

[57] Xinggang Wang, Yongluan Yan, Peng Tang, Xiang Bai, and Wenyu Liu. Revisiting multiple instance neural networks. *Pattern Recognition*, 74:15–24, 2018. 2

[58] Chensu Xie, Hassan Muhammad, Chad M Vanderbilt, Raul Caso, Dig Vijay Kumar Yarlagadda, Gabriele Campanella, and Thomas J Fuchs. Beyond classification: Whole slide tissue histopathology analysis by end-to-end part learning. In *Medical Imaging with Deep Learning*, pages 843–856. PMLR, 2020. 2

[59] Kelvin Xu, Jimmy Ba, Ryan Kiros, Kyunghyun Cho, Aaron Courville, Ruslan Salakhudinov, Rich Zemel, and Yoshua Bengio. Show, attend and tell: Neural image caption generation with visual attention. In *International conference on machine learning*, pages 2048–2057. PMLR, 2015. 2, 3, 5

[60] Quanzeng You, Hailin Jin, Zhaowen Wang, Chen Fang, and Jiebo Luo. Image captioning with semantic attention. In *Proceedings of the IEEE conference on computer vision and pattern recognition*, pages 4651–4659, 2016. 2, 3

[61] Jianbo Yuan, Haofu Liao, Rui Luo, and Jiebo Luo. Automatic radiology report generation based on multi-view image fusion and medical concept enrichment. In *Medical Image Computing and Computer Assisted Intervention – MICCAI 2019*, pages 721–729, 2019. 3

[62] Hongrun Zhang, Yanda Meng, Yitian Zhao, Yihong Qiao, Xiaoyun Yang, Sarah E Coupland, and Yalin Zheng. Dtfd-mil: Double-tier feature distillation multiple instance learning for histopathology whole slide image classification. In *Proceedings of the IEEE/CVF Conference on Computer Vision and Pattern Recognition*, pages 18802–18812, 2022. 1, 2

[63] Zizhao Zhang, Pingjun Chen, Mason McGough, Fuyong Xing, Chunbao Wang, Marilyn Bui, Yuanpu Xie, Manish Sapkota, Lei Cui, Jasreman Dhillon, et al. Pathologist-level interpretable whole-slide cancer diagnosis with deep learning. *Nature Machine Intelligence*, 1(5):236–245, 2019. 1

Supplementary

A. Construction of TCGA-PathoText

In collecting TCGA-PathoText, we use *pytesseract* as the OCR tool to extract word from the PDF files. Then GPT-3.5-turbo is adopted to filter the text.

TCGA-PathoText can be broken down into many subsets according to the disease type, as shown in Table 1. Among these subsets, BRCA contains the most WSI-text pairs.

Subset	Number of pairs
BRCA	1061
KIRC	513
THCA	506
UCEC	504
LUSC	478
LUAD	476
LGG	466
HNSC	450
COAD	450
SKCM	431
STAD	416
PRAD	403
BLCA	386
LIHC	365
CESC	269
SARC	247
PCPG	175
ESCA	156
TGCT	144
THYM	121
OV	106
KICH	94
UVM	80
MESO	75
UCS	57
ACC	56
DLBC	44
CHOL	39

Table 1. Composition of TCGA-PathoText

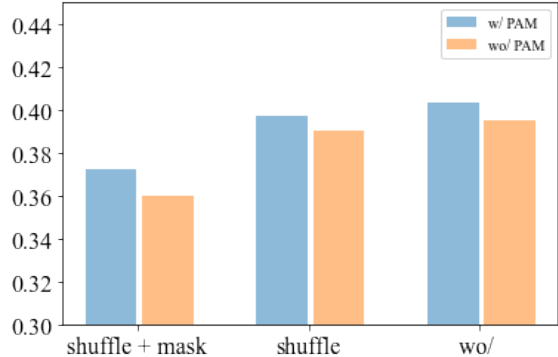


Figure 1. Effect of patch shuffling. We validate our method by distorting the order of the tokens.

	BLEU-1	BLEU-4
Single Layer	0.092	0.377
$3 \times 3 + 5 \times 5 + 7 \times 7$	0.096	0.385
3×3	0.095	0.381
7×7	0.090	0.383
w/o	0.089	0.395
Ours	0.117	0.403

Table 2. Effect of Position-aware Module with different structures. 'Single Layer' represents we only insert the PAM after the final encoder block.

B. Effect of Patch Shuffling

We add noise into the spatial context by shuffling the patches in the training stage. And the test data is not shuffled or masked. The results are shown in Fig. 1. We still use BLEU-1 to measure the generation performance. "shuffle + mask" represents that we shuffle and mask the tokens at the same time. We can observe that PAM improves our model consistently. The improvement can be 4% when the training patches are shuffled and masked.

C. Effect of Position-aware Module

We also modify the structure of the proposed position-aware module to analyze its effectiveness. The related results are

shown in Table 2. Compared with the model without any position-aware modules, we can see that PAM can consistently improve the performance whatever the structure is. And applying convolutional layers with only one type of kernel improves the diagnosis not as well as the combination of different kernels. Furthermore, adding larger kernels equips the model with a larger receptive field to better extract spatial information.